International Journal of Solids and Structures 46 (2009) 3860–3872

Contents lists available at ScienceDirect

International Journal of Solids and Structures

journal homepage: www.elsevier.com/locate/ijsolstr

A fast volume integral equation method for the direct/inverse problem in elastic wave scattering phenomena

Terumi Touhei [a,*], Taku Kiuchi [b,1], Kentaro Iwasaki [c,1]

[a] Department of Civil Engineering, Tokyo University of Science, 2641, Yamazaki Noda City 278-8510, Japan
[b] IBM Japan Ltd., 3-2-12 Roppongi, Minato-ku, Tokyo 106-8711, Japan
[c] System Integrator Corporation, 1-10-1 Numakage, Minami-ku, Saitama City 336-0027, Japan

ARTICLE INFO

Article history:
Received 7 February 2009
Received in revised form 30 May 2009
Available online 23 July 2009

Keywords:
Volume integral equation
Fast method
Forward and inverse scattering problem
Fast Fourier transform
Bi-CGSTAB method
Wavenumber domain formulation

ABSTRACT

A fast method for solving the volume integral equation is introduced for the solution of forward and inverse multiple scattering problems in an elastic 3-D full space. For both forward and inverse scattering analysis, the volume integral equation in the wavenumber domain is used. By means of the discrete Fourier transform, the volume integral equation in the wavenumber domain can be dealt with as a Fredholm equation of the 2nd kind with respect to a non-Hermitian operator on a finite dimensional vector space. The Bi-CGSTAB method is employed to construct the Krylov subspace in the wavenumber domain. The current procedure establishes a fast and simplified method without requiring the derivation of a coefficient matrix. Several numerical results validate the accuracy and effectiveness of the current method for both forward and inverse scattering analysis. According to the numerical results, the reconstruction of inhomogeneities of the wave field is successful, even for multiple scattering of several cubes.

1. Introduction

The analysis of elastic wave propagation and scattering is an important issue in fields such as earthquake engineering, non-destructive testing and exploration for energy resources. It is well recognized that the boundary integral equation method has played an important role in the analysis of both forward and inverse scattering problem since the 1980s. For example, Colton and Kress (1998) provided a survey of a vast number of articles on forward and inverse scattering analyses. They also presented integral equation methods for acoustic and electromagnetic wave propagation, based on the theory of operators (Colton and Kress (1983, 1998)). Recently, Guzina et al. (2003), Fata and Guzina (2004), Guzina and Chikichev (2007) have dealt with inverse scattering problems in elastodynamics.

The type of volume integral equation known as the Lippmann–Schwinger equation (Colton and Kress, 1998) has been an efficient tool for theoretical investigation in the field of the quantum mechanics (see, for example, Ikebe, 1960). Recently, applications of the volume integral equation to scattering analysis have also appeared. For example, De Zaeytijd et al. (2008) presented the MLFMA-FFT method to analyze electro-magnetic waves, and Yang et al. (2008) employed a CG-FFT approach to solve elastic scattering problems. Those methods established a fast algorithm to solve the volume integral equation via a Fast Fourier transform, which is used for efficient calculation of the convolution integral.

This paper presents another fast method for the volume integral equation, applicable to the direct forward and inverse elastic wave scattering problems, which is an extension of the author's approach for an elastic half space (Touhei, 2009). The starting point of the analysis is the volume integral equation in the wavenumber domain, which includes the operators of the Fourier integral and its inverse transforms. By replacing these operators with discrete Fourier transforms, the volume integral equation in the wavenumber domain can be treated as a Fredholm equation of the 2nd kind with a non-Hermitian operator on a finite dimensional vector space. The spatial differential operations with respect to the displacement field are resolved by means of a discrete Fourier transform. The Krylov subspace to approximate the solution of the equation is constructed in the wavenumber domain using the Bi-CGSTAB method and FFT. These points differ from previous volume integral equation methods such as the CG-FFT method (Yang et al., 2008), in which the formulation is carried out in the space domain in terms of particle velocities and stress tensors.

An important property of the volume integral equation in the wavenumber domain is that it separates the scattered wave field from the fluctuation of the medium. This property yields the possibility of inverse scattering analysis. It is true that there are several methods for inverse scattering analysis that make use of the volume integral equation (for example, Kleinman and van den Berg

* Corresponding author. Tel.: +81 4 7122 9629; fax: +81 4 7123 9766.
E-mail address: touhei@rs.noda.tus.ac.jp (T. Touhei).
[1] Formerly graduate student of Tokyo University of Science.

0020-7683/$ - see front matter © 2009 Elsevier Ltd. All rights reserved.
doi:10.1016/j.ijsolstr.2009.07.010

(1992): Colton and Kress (1998)). In these methods, they investigate the relationship between the far field patterns and the fluctuation of the medium in the volume integral equation in the space domain. Under these circumstances, the investigation of the possibility of solving the volume integral equation in the wavenumber domain is also needed for the inverse scattering analysis.

In the following, the definition of the direct forward and inverse scattering problem dealt with in this paper is clarified. After providing an explanation of the properties of the volume integral equation in the wavenumber domain, a fast method for the forward and inverse scattering analyses is provided. Several numerical calculations are presented to validate this formulation.

2. Method for forward and inverse scattering analysis

2.1. Definition of the problem

Fig. 1(a) shows the concept of the problem defined in this paper. A plane incident wave is propagating towards an inhomogeneous region where material properties fluctuate with respect to their reference values. The forward and inverse scattering problems dealt with in this paper can be described as follows:

Definition 1. The forward scattering problem is to determine the scattered wave field from information about the regions of fluctuation, the background structure of the wave field, and the plane incident wave.

Definition 2. The inverse scattering problem is to reconstruct the fluctuated areas from information about the scattered waves, the background structure of the wave field, and the plane incident wave.

The purpose of this section is to provide the basic equations and an integral equation to state the above problems in a mathematical way.

The wave field considered in this paper is 3-D elastic full space, in which a Cartesian coordinate system is employed. A spatial point in the wave field is expressed as:

$$x = (x_1, x_2, x_3) \in \mathbb{R}^3 \tag{1}$$

where the subscript index indicates the component of the vector. The fluctuation of the medium is expressed by the Lamé constants so that:

$$\begin{aligned} &\lambda(x) = \lambda_0 + \tilde{\lambda}(x) \\ &\mu(x) = \mu_0 + \tilde{\mu}(x), \quad (x \in \mathbb{R}^3) \end{aligned} \tag{2}$$

where λ_0 and μ_0 are the background Lamé constants of the wave field, and $\tilde{\lambda}$ and $\tilde{\mu}$ are their fluctuations. The back ground Lamé con-

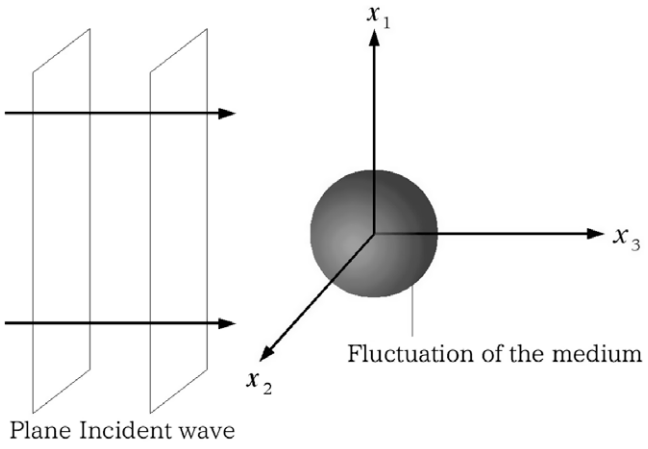

(a) Concept of the analyzed model

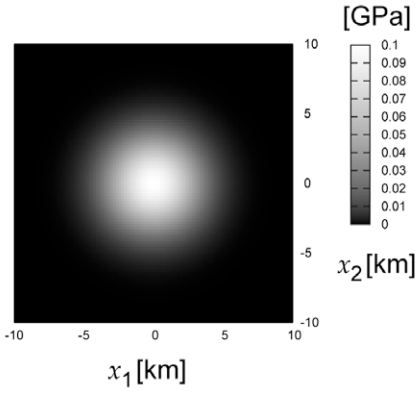

(b) Fluctuations of Lamé constants $\tilde{\lambda}$ and $\tilde{\mu}$ in the $x_1 - x_2$ plane

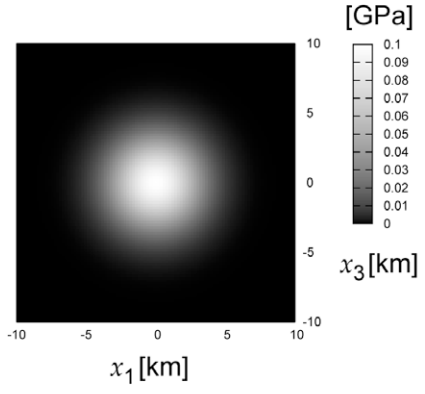

(c) Fluctuations of Lamé constants $\tilde{\lambda}$ and $\tilde{\mu}$ in the $x_1 - x_3$ plane

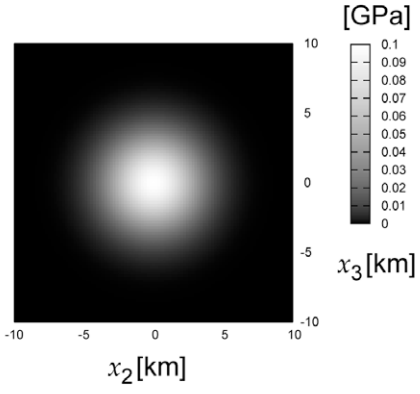

(d) Fluctuations of Lamé constants $\tilde{\lambda}$ and $\tilde{\mu}$ in the $x_2 - x_3$ plane

Fig. 1. Spatial spreads of the fluctuation of the Lamé constants $\tilde{\lambda}$ and $\tilde{\mu}$.

stants are positive and bounded. The magnitudes of the fluctuations in this paper are assumed to satisfy

$$|\tilde{\lambda}(x)| < \lambda_0, \quad |\tilde{\mu}(x)| < \mu_0 \tag{3}$$

Let the time factor of the wave field be $\exp(-i\omega t)$, where ω is the circular frequency and t is the time. Then, the equilibrium equation of the wave field is expressed as:

$$\partial_j \sigma_{ij} + \rho\omega^2 u_i = 0 \tag{4}$$

where σ_{ij} is the stress tensor, ∂_j is the partial differential operator, ρ is the mass density, and u_i is the total displacement field. The subscript indices i and j in Eq. (4) are the components of the Cartesian coordinate system to which the summation convention is applied. The constitutive equation showing the relation between the stress and strain tensors is as follows:

$$\sigma_{ij} = \lambda\delta_{ij}\epsilon_{kk} + 2\mu\epsilon_{ij} \tag{5}$$

where δ_{ij} is the Kronecker delta, and ϵ_{ij} is the strain tensor given by

$$\epsilon_{ij} = (1/2)(\partial_i u_j + \partial_j u_i) \tag{6}$$

Substituting Eqs. (6) and (5) into Eq. (4) yields the following governing equation for the current problem:

$$(L_{ij}(\partial_1, \partial_2, \partial_3) + \delta_{ij}\rho\omega^2)u_j(x) = N_{ij}(\partial_1, \partial_2, \partial_3, x)u_j(x) \tag{7}$$

where $L_{ij}(\partial_1, \partial_2, \partial_3)$ and $N_{ij}(\partial_1, \partial_2, \partial_3, x)$ are the differential operators constructed by the background Lamé constants and their fluctuations, respectively. The explicit forms of the operators L_{ij} and N_{ij} are given by

$$L_{ij}(\partial_1, \partial_2, \partial_3) = (\lambda_0 + \mu_0)\partial_i\partial_j + \mu_0\delta_{ij}\partial_k\partial_k \tag{8}$$

$$N_{ij}(\partial_1, \partial_2, \partial_3, x) = -(\tilde{\lambda}(x) + \tilde{\mu}(x))\partial_i\partial_j - \delta_{ij}\tilde{\mu}(x)\partial_k\partial_k - \partial_i\tilde{\lambda}(x)\partial_j - \delta_{ij}\partial_k\tilde{\mu}(x)\partial_k - \partial_j\tilde{\mu}(x)\partial_i \tag{9}$$

The volume integral equation can now be presented here. Assume the right side of Eq. (7) as the inhomogeneous term for the equation. Then, the solution of Eq. (7) is expressed by the following volume integral equation:

$$u_i(x) = u_i^{(I)}(x) - \int_{\mathbb{R}^3} g_{ij}(x, y)N_{jk}(\partial_1, \partial_2, \partial_3, y)u_k(y)\,dy \tag{10}$$

where $u_i^{(I)}$ and g_{ij} are the plane incident wave and the Green's function, respectively, which satisfy the following equations:

$$(L_{ij}(\partial_1, \partial_2, \partial_3) + \delta_{ij}\rho\omega^2)u_j^{(I)}(x) = 0 \tag{11}$$

$$(L_{ij}(\partial_1, \partial_2, \partial_3) + \delta_{ij}\rho\omega^2)g_{jk}(x, y) = -\delta_{ik}\delta(x - y) \tag{12}$$

Note that $\delta(\cdot)$ in Eq. (12) is the Dirac delta function. It is convenient to express the volume integral equation in terms of the scattered wave field

$$v_i(x) = u_i(x) - u_i^{(I)}(x) \tag{13}$$

which becomes:

$$v_i(x) = -\int_{\mathbb{R}^3} g_{ij}(x, y)N_{jk}(\partial_1, \partial_2, \partial_3, y)u_k^{(I)}(y)\,dy - \int_{\mathbb{R}^3} g_{ij}(x, y)N_{jk}(\partial_1, \partial_2, \partial_3, y)v_k(y)\,dy \tag{14}$$

By means of Eq. (14), the forward and inverse scattering problems can be stated mathematically. The forward scattering problem is to determine v_i after g_{ij}, N_{jk} and $u_k^{(I)}$ have been provided. The inverse scattering problem determines $\tilde{\lambda}$ and $\tilde{\mu}$ in N_{jk} in Eq. (14) after g_{ij}, v_i and $u_k^{(I)}$ have been provided. A method for dealing with Eq. (14) is explained in the remainder of this section.

2.2. The Fourier transform and its application to the volume integral equation

The following Fourier integral and its inverse transforms:

$$(\mathscr{F}u_i)(\xi) = \frac{1}{\sqrt{2\pi}^3}\int_{\mathbb{R}^3} u_i(x)\exp(-ix\cdot\xi)\,dx$$
$$(\mathscr{F}^{-1}\hat{u}_i)(x) = \frac{1}{\sqrt{2\pi}^3}\int_{\mathbb{R}^3} \hat{u}_i(\xi)\exp(ix\cdot\xi)\,d\xi \tag{15}$$

play an important role in the formulation in this paper, where $\xi = (\xi_1, \xi_2, \xi_3) \in \mathbb{R}^3$ is a point in the wavenumber space, $x\cdot\xi$ is the scalar product defined by

$$x\cdot\xi = x_1\xi_1 + x_2\xi_2 + x_3\xi_3 \tag{16}$$

and $\mathscr{F}$ and $\mathscr{F}^{-1}$ are the operators for the Fourier and its inverse transforms, respectively. In the following formulation, the symbol $\hat{}$ attached to a function is used to express the Fourier transform of the function. For example, $\hat{u}_i$ denotes the Fourier transform of u_i. The domain of the operators for $\mathscr{F}$ and $\mathscr{F}^{-1}$ defined in Eq. (15) is assumed to be $L^2(\mathbb{R}^3)$, so that the convergence of the integrals should be understood in the sense of the limit in mean. In the following formulation, the domain of $\mathscr{F}$ and $\mathscr{F}^{-1}$ for the Green's function is assumed to be extended from $L^2(\mathbb{R}^3)$ to the distribution (Hörmander, 1983).

The Fourier transform of the equation for the Green's function defined by Eq. (12) becomes

$$L_{ij}(i\xi_1, i\xi_2, i\xi_3)\hat{g}_{jk}(\xi, y) = -\frac{1}{\sqrt{2\pi}^3}\delta_{ik}\exp(-i\xi\cdot y) \tag{17}$$

Eq. (17) leads to

$$\hat{g}_{ij}(\xi, y) = \frac{1}{\sqrt{2\pi}^3}\exp(-i\xi\cdot y)\hat{h}_{ij}(\xi) \tag{18}$$

where $\hat{h}_{ij}(\xi)$ is expressed by

$$\hat{h}_{ij}(\xi) = \frac{\delta_{ij}}{\mu_0(|\xi|^2 - k_T^2 - i\epsilon)} - \frac{\xi_i\xi_j}{2\mu_0(1-\nu_0)}\frac{1}{(|\xi|^2 - k_T^2 - i\epsilon)(|\xi|^2 - k_L^2 - i\epsilon)} \tag{19}$$

In Eq. (19), ν_0 is the Poisson ratio obtained from the back ground Lamé constants λ_0 and μ_0, k_L and k_T are the wavenumber of the P and S waves obtained from

$$k_L = \frac{\omega}{\sqrt{(\lambda_0 + 2\mu_0)/\rho}}$$
$$k_T = \frac{\omega}{\sqrt{\mu_0/\rho}} \tag{20}$$

$|\xi|^2$ is given by

$$|\xi|^2 = \xi_1^2 + \xi_2^2 + \xi_3^2 \tag{21}$$

and ϵ is the infinitesimally small positive number.

Now, let us investigate the Fourier transform of function w_i given in the form

$$w_i(x) = \int_{\mathbb{R}^3} g_{ij}(x, y)f_j(y)\,dy \tag{22}$$

to obtain the Fourier transform of the volume integral equation. Note that $f_j(y)$ is in $\mathscr{S}(\mathbb{R}^3)$, that is, the space of rapidly decreasing functions (Reed and Simon, 1975). An interchange of the order of integration yields

$$\hat{w}_i(\xi) = \frac{1}{\sqrt{2\pi}^3}\int_{\mathbb{R}^3}\left[\int_{\mathbb{R}^3} g_{ij}(x,y) f_j(y)\,dy\right]\exp(-ix\cdot\xi)\,dx = \hat{h}_{ij}(\xi)\frac{1}{\sqrt{2\pi}^3}\int_{\mathbb{R}^3} f_j(y)\exp(-i\xi\cdot y)\,dy = \hat{h}_{ij}(\xi)\hat{f}_j(\xi) \tag{23}$$

In particular, the Fourier transform of w_i can be separated into the product of $\hat{h}_{ij}$ and $\hat{f}_j$. Based on literature (Hörmander, 1983), f_j can be extended to distributions with compact support. According to Eq. (23), the Fourier transform of the volume integral equation shown in Eq. (14) becomes:

$$\hat{v}_i(\xi) = -\hat{h}_{ij}(\xi)(\mathscr{F}N_{jk}u_k^{(I)})(\xi) - \hat{h}_{ij}(\xi)(\mathscr{F}N_{jk}\mathscr{F}^{-1}\hat{v}_k)(\xi) \tag{24}$$

In the case where an explicit form of the plane incident wave is provided, $N_{jk}u_k^{(I)}$ shown in the right side of Eq. (24) can be simplified. As an example, a plane incident pressure (P) wave propagating along the x_3 axis has the following form:

$$u_i^{(I)}(x) = a\partial_i \exp(ik_L x_3) \tag{25}$$

where a is the amplitude of the P wave potential. In this case, $N_{jk}u_k^{(I)}$ can be expressed as

$$N_{jk}u_k^{(I)}(x) = q_j(x)\exp(i\xi_p\cdot x) \tag{26}$$

where

$$\begin{aligned} q_1(x) &= ak_L^2\partial_1\tilde{\lambda}(x)\\ q_2(x) &= ak_L^2\partial_2\tilde{\lambda}(x)\\ q_3(x) &= ak_L^2(\partial_3 + ik_L)(\tilde{\lambda}(x) + 2\tilde{\mu}(x)) \end{aligned} \tag{27}$$

Note that ξ_p is the wavenumber vector of the plane incident wave whose components are:

$$\xi_p = (0,0,k_L) \tag{28}$$

As a result, Eq. (24) can be rewritten as

$$\hat{v}_i(\xi) = -\hat{h}_{ij}(\xi)\hat{q}_j(\xi-\xi_p) - \hat{h}_{ij}(\xi)(\mathscr{F}N_{jk}\mathscr{F}^{-1}\hat{v}_k)(\xi) \tag{29}$$

A method for forward and inverse scattering analysis is developed in the following based on Eq. (29).

2.3. Method for forward scattering analysis

At this point, let us rewrite Eq. (29) in the following form:

$$\hat{v}_i(\xi) = \hat{f}_i(\xi) - \mathscr{A}_{ik}\hat{v}_k \tag{30}$$

where $\hat{f}_i$ is given by

$$\hat{f}_i(\xi) = -\hat{h}_{ij}(\xi)\hat{q}_j(\xi-\xi_p) \tag{31}$$

which can be treated as a given function and $\mathscr{A}_{ik}$ is the linear operator such that

$$\mathscr{A}_{ik} = \hat{h}_{ij}(\xi)\mathscr{F}N_{jk}\mathscr{F}^{-1} \tag{32}$$

Eq. (30) shows clearly a Fredholm integral equation of the second kind, in which the linear operator is constructed by the multiplication operator $\hat{h}_{ij}$, the Fourier and its inverse transforms, and the differential operator N_{jk}. For the actual numerical calculations in this paper, the Fourier and its inverse transforms are dealt with by means of the discrete Fourier transform. Naturally, the discrete Fourier transform is evaluated by means of an FFT. Let us denote the operators for the discrete Fourier transforms as $\mathscr{F}_D$ and $\mathscr{F}_D^{-1}$. For the operators $\mathscr{F}_D$ and $\mathscr{F}_D^{-1}$, the subsets in $\mathbb{R}^3$ below are defined as follows:

$$D_x = \{(n_1\Delta x_1, n_2\Delta x_2, n_3\Delta x_3) | n_1\in\mathbb{N}_1, n_2\in\mathbb{N}_2, n_3\in\mathbb{N}_3\}\subset\mathbb{R}^3 \tag{33}$$

$$D_\xi = \{(n_1\Delta\xi_1, n_2\Delta\xi_2, n_3\Delta\xi_3) | n_1\in\mathbb{N}_1, n_2\in\mathbb{N}_2, n_3\in\mathbb{N}_3\}\subset\mathbb{R}^3 \tag{34}$$

These subsets define a finite number of grid points, where Δx_j, $(j=1,2,3)$ is the interval of the grid in the space domain, $\Delta\xi_j$, $(j=1,2,3)$ is the interval of the grid in the wavenumber space, and $\mathbb{N}_1$, $\mathbb{N}_2$ and $\mathbb{N}_3$ are sets of integers defined by

$$\begin{aligned} \mathbb{N}_1 &= \{n | -N_1/2 \leqslant n < N_1/2\}\\ \mathbb{N}_2 &= \{n | -N_2/2 \leqslant n < N_2/2\}\\ \mathbb{N}_3 &= \{n | -N_3/2 \leqslant n < N_3/2\} \end{aligned} \tag{35}$$

where (N_1, N_2, N_3) defines the number of grid points in $\mathbb{R}^3$. For the discrete Fourier transform, note that there is a relation between Δx_j and $\Delta\xi_j$ such that

$$\Delta x_j\Delta\xi_j = \frac{2\pi}{N_j}, \quad (j=1,2,3) \tag{36}$$

The explicit form of the discrete Fourier and its inverse transforms are expressed as

$$\begin{aligned} (\mathscr{F}_D u_{(D)})(\xi^{(l)}) &= \frac{\Delta x}{\sqrt{2\pi}^3}\sum_{k\in\mathbb{N}_1\times\mathbb{N}_2\times\mathbb{N}_3} u_{(D)}(x^{(k)})\exp(-ix^{(k)}\cdot\xi^{(l)})\\ (\mathscr{F}_D^{-1}\hat{u}_{(D)})(x^{(k)}) &= \frac{\Delta\xi}{\sqrt{2\pi}^3}\sum_{l\in\mathbb{N}_1\times\mathbb{N}_2\times\mathbb{N}_3} \hat{u}_{(D)}(\xi^{(l)})\exp(ix^{(k)}\cdot\xi^{(l)}) \end{aligned} \tag{37}$$

where Δx and $\Delta\xi$ are denoted by

$$\Delta x = \Delta x_1\Delta x_2\Delta x_3, \quad \Delta\xi = \Delta\xi_1\Delta\xi_2\Delta\xi_3 \tag{38}$$

and $x^{(k)}$ and $\xi^{(l)}$ expressed by

$$x^{(k)} = \left(x_1^{(k)}, x_2^{(k)}, x_3^{(k)}\right), \quad \xi^{(l)} = \left(\xi_1^{(l)}, \xi_2^{(l)}, \xi_3^{(l)}\right) \tag{39}$$

are the points in D_x of the kth grid and in D_ξ of the lth grid, respectively. In addition, u_D and $\hat{u}_D$ are the discrete functions defined on the grids D_x and D_ξ.

Based on the discrete Fourier transform, a calculation for the derivative of a function is made possible. For example, $\partial_j f(x)$ is expressed by

$$\partial_j f(x) = (\mathscr{F}_D^{-1}(i\xi_j\mathscr{F}_D f))(x), \quad x\in D_x, \ \ \xi\in D_\xi \tag{40}$$

Therefore, treatments for the operator N_{jk} are also made possible by the discrete Fourier transform. Let $N_{(D)jk}$ be the discretization of the operator for N_{jk} by means of the discrete Fourier transform. Then, the discretization for the operator $\mathscr{A}_{ij}$ is defined by

$$\mathscr{A}_{(D)ik} = \hat{h}_{ij}(\xi)\mathscr{F}_D N_{(D)jk}\mathscr{F}_D^{-1} \tag{41}$$

As a result of the discretization, Eq. (30) becomes

$$\hat{v}_{(D)i}(\xi) = \hat{f}_{(D)i}(\xi) - \mathscr{A}_{(D)ij}\hat{v}_{(D)j}(\xi) \quad (\xi\in D_\xi) \tag{42}$$

The domain and range of the linear operator in Eq. (41) are in the set of functions defined on finite number of grids in the wavenumber space D_ξ. Namely, the domain and range for the operator are finite dimensional vector spaces. Note that the operator $N_{(D)jk}$ included in $\mathscr{A}_{(D)ij}$ is bounded since the differential operations are approximated by the discrete Fourier transform. In the case that the domain and range of operator are finite dimensional vector spaces, the operator has matrix representations (Kato, 1980). Based on this result, a treatment for the linear algebraic equation such as the Krylov subspace iteration method (Barrett et al., 1994) is applicable to Eq. (42). It is known that the Krylov subspace iteration methods have been developed for systems of algebraic equations in matrix form:

$$A\boldsymbol{x} = \boldsymbol{b} \tag{43}$$

where A is the matrix, $\boldsymbol{x}$ and $\boldsymbol{b}$ are unknown and given vectors, respectively. The Krylov subspace is defined by

$$K_m = \text{span}\,\{\boldsymbol{b}, A\boldsymbol{b}, A^2\boldsymbol{b}\ldots, A^m\boldsymbol{b}\} \tag{44}$$

where m is the number of iterations. The Krylov subspace iteration method determines the coefficients of the recurrence formula to approximate the solution from the orthonormal basis of K_m during the iterative procedure. Note that matrix A can be regarded as the linear transform on a finite dimensional vector space. In this aspect, the construction of the Krylov subspace is possible, even if the linear transform is constituted by the discrete Fourier transforms. Namely, it is possible to solve Eq. (42) by the Krylov subspace iteration method, where the construction of the Krylov subspace is carried out by FFT. As a result, a fast method for the volume integral equation without the derivation of the matrix is expected to be established. The current method is also expected to use less computer memory for numerical analysis. Since the operator $\mathscr{A}_{(D)ij}$ is non-Hermitian due to the presence of $N_{(D)jk}$, the Bi-CGSTAB method (Barrett et al., 1994) is selected to solve Eq. (42). The algorithm for the Bi-CGSTAB method is shown in Fig. 2, where (n+1) denotes the parameter for the number of iterations. In the following numerical examples, the number of iterations will be discussed by means of the parameter (n+1).

2.4. Method for inverse scattering analysis

According to Eq. (27) the explicit form of $\hat{q}_j(\xi-\xi_p)$ shown in the first term of the right side of Eq. (29) becomes:

$$\begin{aligned}\hat{q}_1(\xi-\xi_p) &= ak_L^2 i\xi_1 \hat{\tilde{\lambda}}(\xi-\xi_p)\\ \hat{q}_2(\xi-\xi_p) &= ak_L^2 i\xi_2 \hat{\tilde{\lambda}}(\xi-\xi_p)\\ \hat{q}_3(\xi-\xi_p) &= ak_L^2 i\xi_3(\hat{\tilde{\lambda}}(\xi-\xi_p)+2\hat{\tilde{\mu}}(\xi-\xi_p))\end{aligned} \tag{45}$$

It is found from Eq. (45) that $\hat{q}_j$ is the function describing the fluctuation of the medium. Therefore, the inverse scattering analysis becomes possible if $\hat{q}_j$ is obtained from Eq. (29) after the scattered wave field $\hat{v}_i$ and the background structure of the wave field represented by $\hat{h}_{ij}$ have been provided. We introduce the vector Q_i such that $q_i(x)=ak_L^3\lambda_0 Q_i(x)$ to obtain the equation for the inverse scattering analysis in dimensionless form. Let us multiply both sides of Eq. (29) by $(-\hat{h}_{ij}^{-1}/(a\lambda_0 k_L^3))$, which leads to

$$\hat{\gamma}_j(\xi) = \widehat{Q}_j(\xi-\xi_p) + \frac{1}{ak_L^3\lambda_0}(\mathscr{F}N_{jk}\mathscr{F}^{-1}\hat{v}_k)(\xi) \tag{46}$$

where $\hat{\gamma}_j$ is defined by

$$\hat{\gamma}_j(\xi) = -\hat{h}_{ji}^{-1}(\xi)\hat{v}_i(\xi)/(a\lambda_0 k_L^3) \tag{47}$$

Compute $\boldsymbol{r}_0=\boldsymbol{b}-A\boldsymbol{x}_0$ for some initial guess $\boldsymbol{x}_0$,
Choose $\tilde{\boldsymbol{r}}$ such that $(\tilde{\boldsymbol{r}},\boldsymbol{r}_0)\neq 0$, *e.g.*, $\tilde{\boldsymbol{r}}=\boldsymbol{r}_0$,
for $n=0,1,\cdots$
  if $n=0$
    $\boldsymbol{p}_n=\boldsymbol{r}_n$,
  else
    $\beta_{n-1}=\frac{\alpha_{n-1}}{\zeta_{n-1}}\cdot\frac{(\tilde{\boldsymbol{r}},\boldsymbol{r}_n)}{(\tilde{\boldsymbol{r}},\boldsymbol{r}_{n-1})}$,
    $\boldsymbol{p}_n=\boldsymbol{r}_n+\beta_{n-1}(\boldsymbol{p}_{n-1}-\zeta_{n-1}A\boldsymbol{p}_{n-1})$,
  end if
  $\alpha_n=\frac{(\tilde{\boldsymbol{r}},\boldsymbol{r}_n)}{(\tilde{\boldsymbol{r}},A\boldsymbol{p}_n)}$,
  $\boldsymbol{s}=\boldsymbol{r}_n-\alpha_n A\boldsymbol{p}_n$,
  check the norm of $\boldsymbol{s}$; if small enough : set $\boldsymbol{x}_{n+1}=\boldsymbol{x}_n+\alpha_n\boldsymbol{p}_n$ and stop
  $\zeta_n=\frac{(A\boldsymbol{s},\boldsymbol{s})}{(A\boldsymbol{s},A\boldsymbol{s})}$,
  $\boldsymbol{x}_{n+1}=\boldsymbol{x}_n+\alpha_n\boldsymbol{p}_n+\zeta_n\boldsymbol{s}$,
  $\boldsymbol{r}_{n+1}=\boldsymbol{s}-\zeta_n A\boldsymbol{s}$,
  if $\|\boldsymbol{r}_{n+1}\|/\|\boldsymbol{b}\|>\epsilon_r$; **continue**,
  (for continuation it is necessary that $\zeta_n\neq 0$)
end

Fig. 2. Algorithm for the Bi-CGSTAB method.

Next, let the second term of Eq. (46) be modified, thus:

$$\frac{1}{ak_L^3\lambda_0}\mathscr{F}N_{jk}\mathscr{F}^{-1}\hat{v}_k(\xi) = \mathscr{F}M_{jk}\mathscr{F}^{-1}\widehat{Q}_k(\xi) \tag{48}$$

where M_{jk} is the differential operator determined by the scattered wave field. The remainder of this section is on how to obtain an explicit form for M_{jk}, so that Eq. (46) can be used for obtaining $\widehat{Q}$, which makes an estimation for fluctuation of the medium possible. To obtain the explicit form for M_{jk}, define $\alpha_j=N_{jk}v_k$, which can be expressed as

$$\alpha_j = -(\tilde{\lambda}+\tilde{\mu})\partial_j\Delta_v - \tilde{\mu}\eta_j - (\partial_j\tilde{\lambda})\Delta_v - 2(\partial_k\tilde{\mu})\epsilon_{kj} \tag{49}$$

where Δ_v and η_j are defined by

$$\begin{aligned}\Delta_v &= \partial_l v_l\\ \eta_j &= (\partial_1^2+\partial_2^2+\partial_3^2)v_j\end{aligned} \tag{50}$$

and ϵ_{jk} is the strain tensor due to the scattered wave field defined by Eq. (6). Let the separation of the fluctuation of the medium and the scattered wave field for α_j be denoted by

$$\alpha_j = -m_{jk}p_k \tag{51}$$

where p_k is the state vector for the fluctuation of the medium whose components are

$$p_1=\partial_1\tilde{\lambda}(x)/k_L,\quad p_2=\tilde{\lambda}(x),\quad p_3=\tilde{\mu}(x) \tag{52}$$

and m_{jk} is the differential operator including the effects of the scattered wave field so that

$$[m_{jk}] = \begin{bmatrix} k_L\Delta_v & \partial_1\Delta_v & \partial_1\Delta_v+\eta_1+2\epsilon_{1l}\partial_l\\ 0 & \Delta_v\partial_2+\partial_2\Delta_v & \partial_2\Delta_v+\eta_2+2\epsilon_{2l}\partial_l\\ 0 & \Delta_v\partial_3+\partial_3\Delta_v & \partial_3\Delta_v+\eta_3+2\epsilon_{3l}\partial_l\end{bmatrix} \tag{53}$$

Likewise, let the separation of the fluctuation of the medium and the scattered wave field for Q_j defined by Eq. (27) be denoted by

$$Q_j = \kappa_{jk}p_k \tag{54}$$

where κ_{jk} is also the operator including the effects of the scattered wave field so that:

$$[\kappa_{jk}] = \frac{1}{k_L\lambda_0}\begin{bmatrix} k_L & 0 & 0\\ 0 & \partial_2 & 0\\ 0 & (\partial_3+ik_L) & 2(\partial_3+ik_L)\end{bmatrix} \tag{55}$$

According to Eqs. (54) and (55), the formal representation of the relation between p_j and Q_j becomes

$$p_j = s_{jk}Q_k \tag{56}$$

where s_{jk} is the inverse of κ_{jk} whose components are

$$[s_{jk}] = \lambda_0 k_L\begin{bmatrix} k_L^{-1} & 0 & 0\\ 0 & \partial_2^{-1} & 0\\ 0 & -(1/2)\partial_2^{-1} & -(1/2)(\partial_3+ik_L)^{-1}\end{bmatrix} \tag{57}$$

Based on Eqs. (51) and (54), the following relation can be derived:

$$\alpha_j = N_{jk}v_k = -m_{jk}p_k = -m_{jk}s_{kl}Q_l \tag{58}$$

As a result, the operator M_{jk} defined by Eq. (48) can be constructed as follows:

$$M_{jl} = -\frac{1}{ak_L^3\lambda_0}m_{jk}s_{kl} \tag{59}$$

By means of the operator, Eq. (46) is modified into

$$\hat{\gamma}_i(\xi) = \widehat{Q}_i(\xi - \xi_p) + (\mathscr{F} M_{ij} \mathscr{F}^{-1}) \widehat{Q}_j(\xi) \tag{60}$$

At this point, we have two tasks for Eq. (60). One is to modify Eq. (60) into the form of a Fredholm equation of the second kind. The other goal is to clarify the treatment of the operator s_{jk}, which includes ∂_2^{-1} and $(\partial_3 + ik_L)^{-1}$. To modify Eq. (60) into a Fredholm equation of a second kind, the shift operator $S(\xi_p)$ defined by

$$S(\xi_p)\widehat{Q}(\xi - \xi_p) = \widehat{Q}(\xi) \tag{61}$$

is introduced. An explicit form of the shift operator is possible in terms of the Fourier transform, so that

$$S(\xi_p) = \mathscr{F} \exp(ix \cdot \xi_p) \mathscr{F}^{-1} \tag{62}$$

Application of the shift operator to both sides of Eq. (60) leads to

$$S(\xi_p)\hat{\gamma}_i(\xi) = \widehat{Q}_i(\xi) + (\mathscr{F} \exp(ix \cdot \xi_p) M_{ij} \mathscr{F}^{-1} \widehat{Q}_j)(\xi) \tag{63}$$

which clearly has the form of a Fredholm equation of the second kind.

To clarify the treatments of ∂_2^{-1} in s_{jk}, consider the following equation:

$$\partial_2 u(x) = f(x), \quad f \in \mathscr{S}(\mathbb{R}^3) \tag{64}$$

Formally, it is possible to write the solution of the equation as

$$u(x) = \partial_2^{-1} f(x) = \int_{-\infty}^{\infty} H(x_2 - x_2') f(x_1, x_2', x_3)\, dx_2' \tag{65}$$

where H is the unit step function. It is clear that $H \in \mathscr{S}'(\mathbb{R})$, where $\mathscr{S}'$ is the set of tempered distributions (Reed and Simon, 1975). Therefore, the Fourier transform of H is defined by

$$\begin{aligned} \int_{-\infty}^{\infty} \widehat{H}(\xi_2)\varphi(\xi_2)\, d\xi_2 &= \int_{-\infty}^{\infty} H(x_2)\hat{\varphi}(x_2)\, dx_2 = \int_0^{\infty} \hat{\varphi}(x_2)\, dx_2 \\ &= \lim_{R\to\infty} \int_0^R \hat{\varphi}(x_2)\, dx_2 \end{aligned} \tag{66}$$

where $\varphi \in \mathscr{S}$. The last term of Eq. (66) yields,

$$\begin{aligned} \sqrt{2\pi}\int_0^R \hat{\varphi}(x_2)dx_2 &= \int_0^R \int_{-\infty}^{\infty} \varphi(\xi_2)\exp(-ix_2\xi_2)\, d\xi_2 dx_2 \\ &= i\int_{-\infty}^{\infty} e^{-iR\xi_2} \frac{\varphi(\xi_2) - \varphi(0)}{\xi_2} d\xi_2 + i\varphi(0) \\ &\times \int_{-\infty}^{\infty} \frac{e^{-iR\xi_2} - 1}{\xi_2} d\xi_2 - i\int_{-\infty}^{\infty} \frac{\varphi(\xi_2) - \varphi(0)}{\xi_2} d\xi_2 \end{aligned} \tag{67}$$

As a result, the Fourier transform of H can be expressed as

$$\widehat{H}(\xi_2) = -\frac{i}{\sqrt{2\pi}}\left(\text{p.v.}\frac{1}{\xi_2} + i\pi\delta(\xi_2)\right) \tag{68}$$

because of the following results:

$$\int_{-\infty}^{\infty} e^{-iR\xi} \frac{\varphi(\xi_2) - \varphi(0)}{\xi_2}\, d\xi \to 0, \quad (R \to \infty) \tag{69}$$

$$i\varphi(0)\int_{-T}^{T} \frac{e^{-iR\xi_2} - 1}{\xi_2}\, d\xi_2 \to \pi\varphi(0), \quad (T \to \infty) \tag{70}$$

$$-i\int_{-\infty}^{\infty} \frac{\varphi(\xi_2) - \varphi(0)}{\xi_2}\, d\xi_2 = -i\ \text{p.v.}\int_{-\infty}^{\infty} \frac{\varphi(\xi_2)}{\xi_2}\, d\xi_2 \tag{71}$$

where p.v. denotes Cauchy's principal value. Eq. (68) can also be expressed as (Friedlander and Joshi, 1998),

$$\widehat{H}(\xi_2) = \frac{1}{\sqrt{2\pi}} \frac{1}{i\xi_2 + \epsilon} \tag{72}$$

and therefore, the Fourier transform for $u(x)$ in Eq. (65) becomes

$$\hat{u}(\xi) = \frac{1}{i\xi_2 + \epsilon}\hat{f}(\xi) \tag{73}$$

The treatment for ∂_2^{-1} is resolved by means of Eq. (73), which is represented by

$$\partial_2^{-1} f = \mathscr{F}^{-1} \frac{1}{i\xi_2 + \epsilon} \mathscr{F} f \tag{74}$$

Likewise, we obtain

$$(\partial_3 + ik_L)^{-1} f = \int_{-\infty}^{\infty} H(x_3 - x_3') \exp(ik_L(x_3 - x_3'))f(x_1, x_2, x_3')\, dx_3' \tag{75}$$

which yields

$$(\partial_3 + ik_L)^{-1} f = \mathscr{F}^{-1} \frac{1}{i\xi_3 + ik_L + \epsilon} \mathscr{F} f \tag{76}$$

As can be seen from Eqs. (74) and (76), ∂_2^{-1} and $(\partial_3 + ik_L)^{-1}$ in the operator s_{ij} can be dealt with and resolved in terms of the Fourier transform. As a result of the above procedure, the treatments of the differential operator M_{ij} defined by Eq. (48) can also be handled by the Fourier transform. After all, as in the formulation for the forward scattering problem, Eq. (63) can be discretized into the following form:

$$S_D(\xi_p)\hat{\gamma}_{(D)i}(\xi) = \widehat{Q}_{(D)i}(\xi) + \mathscr{B}_{(D)ij}\widehat{Q}_{(D)j}, \quad \xi \in D_\xi \tag{77}$$

where $\mathscr{B}_{(D)ij}$ is the operator expressed by

$$\mathscr{B}_{(D)ij} = \mathscr{F}_D \exp(ix \cdot \xi_p) M_{(D)ij} \mathscr{F}_D^{-1} \tag{78}$$

The Krylov subspace iteration technique is also applied to Eq. (77) in the analysis. As a result of the above procedure, a fast method for the analysis of the inverse scattering is expected to be established.

3. Numerical examples

3.1. Verification of the method for the volume integral equation

As the first numerical example in this paper, we examine the accuracy of the current method by calculating the solution to a simple forward scattering problem. The region of fluctuation for the current model is assumed to have spherical symmetry, which enables us to compare the current solution using a spherical harmonics expansion. The fluctuations of Lamé constants having spherical symmetry for the numerical model are set as

$$\begin{aligned} \tilde{\lambda}(x) &= A_\lambda \exp\left(-\zeta_\lambda |x|^2\right) \\ \tilde{\mu}(x) &= A_\mu \exp\left(-\zeta_\mu |x|^2\right), \quad (x \in \mathbb{R}^3) \end{aligned} \tag{79}$$

where $A_\lambda, A_\mu, \zeta_\lambda$ and ζ_μ are the parameters for describing the amplitudes and spatial spreads of the fluctuations.

To construct a solution for the wave problem by means of spherical harmonics, the following Stokes–Helmholtz decomposition, making use of the spherical coordinate system (r, θ, φ), is employed:

$$\boldsymbol{u}(x) = \nabla\Phi + \nabla \times \nabla \times (r\Psi, 0, 0) + \nabla \times (rX, 0, 0) \tag{80}$$

where $\boldsymbol{u}$ is the displacement vector, ∇ is the gradient operator and Φ, Ψ and X are the potentials for the P, SV and SH waves, respectively. The spherical harmonic expansions for these potentials are as follows:

$$\begin{aligned} \Phi(r,\theta,\varphi) &= \sum_{n=0}^{\infty} P_n(\cos\theta)[\alpha_n^{\uparrow}(r)h_n^{(1)}(\kappa_L r) + \alpha_n^{\downarrow}(r)h_n^{(2)}(\kappa_L r)] \\ \Psi(r,\theta,\varphi) &= \sum_{n=0}^{\infty} P_n(\cos\theta)[\beta_n^{\uparrow}(r)h_n^{(1)}(\kappa_T r) + \beta_n^{\downarrow}(r)h_n^{(2)}(\kappa_T r)] \\ X(r,\theta,\varphi) &= \sum_{n=0}^{\infty} P_n(\cos\theta)[\gamma_n^{\uparrow}(r)h_n^{(1)}(\kappa_T r) + \gamma_n^{\downarrow}(r)h_n^{(2)}(\kappa_T r)] \end{aligned} \tag{81}$$

where P_n denote Legendre polynomials, $h_n^{(\tau)}, (\tau = 1, 2)$ is the spherical Hankel function of nth order, α_n, β_n and γ_n are the functions for

r, whose superscript $\uparrow$ and $\downarrow$ indicate the out-going and in-coming waves, respectively, and κ_T and κ_L are the S and P wavenumbers, respectively for the scattered wave field. The functions α_n, β_n and γ_n are determined by the governing equation, the radiation condition, the boundedness of the wave field at the origin of the wave field, and the potential of the incident P wave propagating along the x_3 axis, which can be expanded as

$$\exp(ik_L x_3) = \sum_{n=0}^{\infty}(2n+1)i^n j_n(k_L r)P_n(\cos\theta) \tag{82}$$

where k_L is the wavenumber of the P wave for the background structure of the wave field, and j_n is a spherical Bessel function of the first kind of nth order.

For the numerical analysis, the parameters for describing the fluctuations are set as $A_\lambda = A_\mu = 0.1$ GPa and $\zeta_\lambda = \zeta_\mu = 0.1\ \mathrm{km}^{-2}$. The background structure of the wave field for the Lamé constants is set such that $\lambda_0 = 4$ GPa, $\mu_0 = 2$ GPa and the mass density is set at $\rho = 2\ \mathrm{g/cm}^3$. The background velocity of the P and S waves are 2 and 1 km/s, respectively. The analyzed frequency $f = 1$ Hz, the amplitude of the potential for the incident P wave is $A = 1.0\times 10^5\ \mathrm{cm}^2$, intervals of the grids in the space domain for the discrete Fourier transform are set by $\Delta x_j = 0.25$ (km), $(j = 1,2,3)$ and the numbers for the grids are set as $N_j = 256$ $(j = 1,2,3)$. As a result, the intervals of the grid in the wavenumber space become $\Delta\xi_j = 2\pi/(N_j \times \Delta x_j) \approx 0.098\ \mathrm{km}^{-1}$. In addition, ϵ for Green's function in the wavenumber domain shown in Eq. (19) is set to 0.2.

Fig. 1(b)–(d) show the spatial spread of the fluctuation in the $x_1 - x_2, x_1 - x_3$ and $x_2 - x_3$ planes for the numerical model, in which the gradual variation of Lamé constants can be seen inside a circle of radius 6 km. This radius of the region of fluctuations is three times larger than the P wave length of 2 km.

Fig. 3 shows a comparison of the current solution with the spherical harmonics expansion for the scattered displacements fields at the $x_3 = 4$ km plane and along the x_3 axis, respectively.

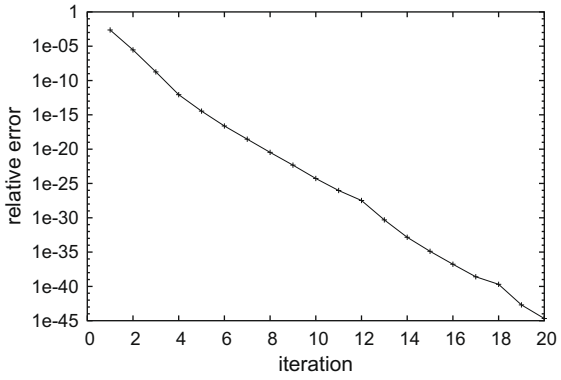

Fig. 4. Convergence of the solution by the Bi-CGSTAB method.

It can be seen from Fig. 3(b) that the amplitudes of the backward scattering are very small. The scattering waves are amplified inside the region of fluctuation and tend to propagate to the forward region. According to the figure, these two solutions are in good agreement. These numerical results validate the accuracy of the current formulation. As mentioned before, the Bi-CGSTAB method is selected here from the Krylov subspace iteration methods. The relation between the relative error and the number of iterations during the iterative process is shown in Fig. 4. The relative error ϵ_r during the iteration is defined as

$$\epsilon_r = \frac{\|\hat{\boldsymbol{v}}_{(D)i}(\xi) + \mathscr{A}_{(D)ij}\hat{\boldsymbol{v}}_{(D)j}(\xi) - \hat{\boldsymbol{f}}_{(D)i}(\xi)\|}{\|\hat{\boldsymbol{f}}_{(D)j}(\xi)\|} \tag{83}$$

which is equivalent to $\|\boldsymbol{r}_{(n+1)}\|/\|\boldsymbol{b}\|$ shown in Fig. 2, where n is the number of iteration. The rapid decrease of the relative error can be seen in Fig. 4, which indicates that only two iterations resulted

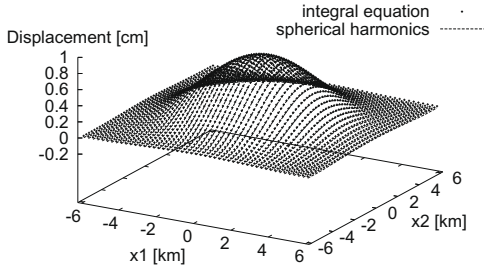

(a) Comparison of displacement at the $x_3 = 4$ km plane.

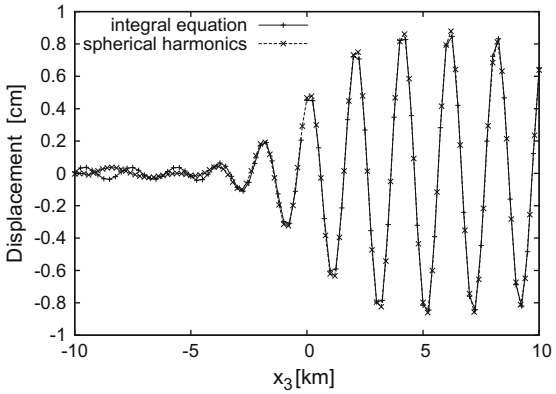

(b) Comparison of displacement along the x_3 axis.

Fig. 3. Comparison of current solution with the spherical harmonics expansion.

in a relative error less than 1.0×10^{-5}. The CPU time needed for the two iterations was only 2 min, for which an AMD Opteron 2.4 GHz processor and the ACML library for FFT (http://developer.amd.com/cpu/Libraries/acml) was used.

3.2. Analysis of multiple scattering due to smooth fluctuations

Next, we investigate a multiple scattering problem arising from smooth fluctuations of the wave field. The smoothness of the

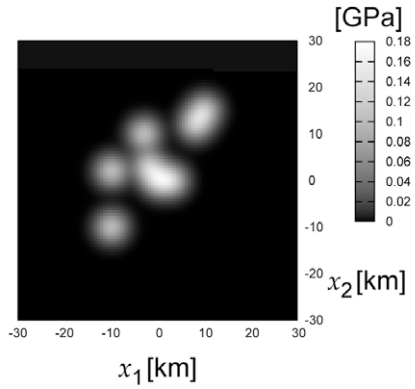

(a) Fluctuations of Lamé constants $\tilde{\lambda}$ and $\tilde{\mu}$ in the $x_1 - x_2$ plane.

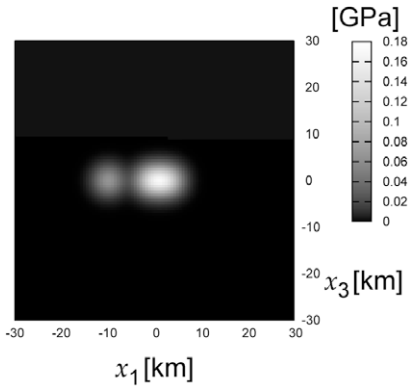

(b) Fluctuations of Lamé constants $\tilde{\lambda}$ and $\tilde{\mu}$ in the $x_1 - x_3$ plane.

Fig. 5. Analyzed model of smooth fluctuations.

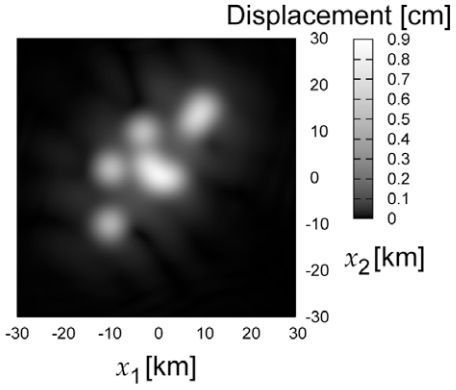

(a) Amplitudes of scattered waves in the $x_1 - x_2$ plane.

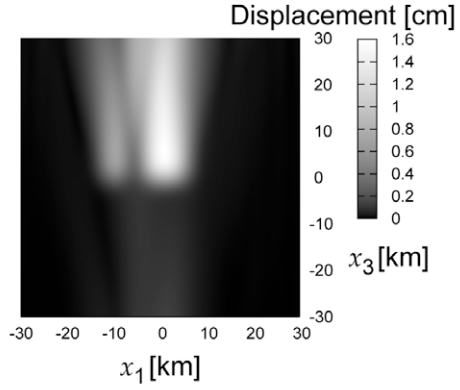

(b) Amplitudes of the scattered waves in the $x_1 - x_3$ plane.

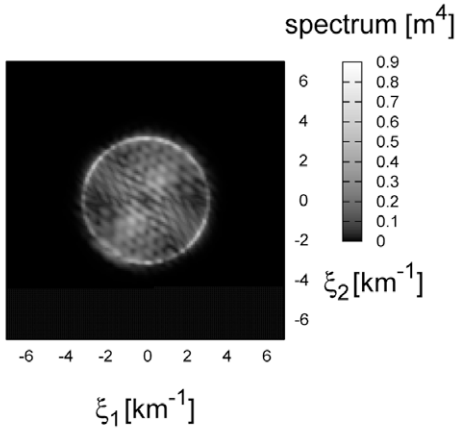

(c) Wavenumber spectrum of the scattered waves in the $\xi_1 - \xi_2$ plane.

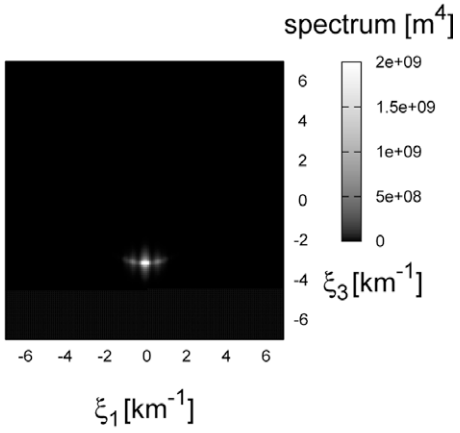

(d) Wavenumber spectrum of the scattered waves in the $\xi_1 - \xi_3$ plane.

Fig. 6. Results of the forward scattering analysis due to smooth fluctuations.

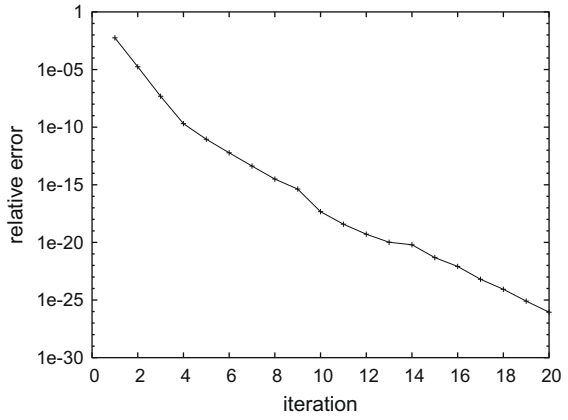

Fig. 7. Convergence of the solution for the forward scattering analysis due to smooth fluctuations by the Bi-CGSTAB method.

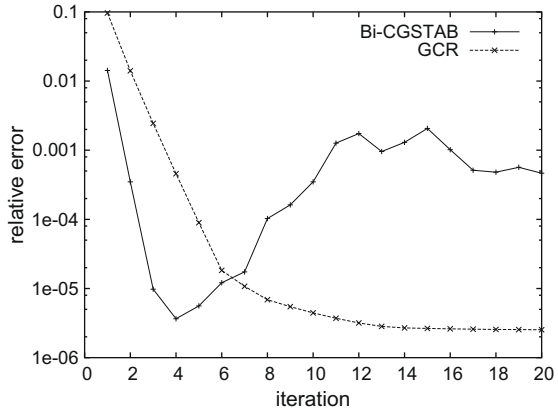

Fig. 9. Convergence of the solution for the inverse scattering analysis due to smooth fluctuation.

fluctuations implies that they have continuous spatial derivatives. The fluctuations in the $x_1 - x_2$ and $x_1 - x_3$ planes are shown in Fig. 5, where the maximum amplitudes of $\tilde{\lambda}$ and $\tilde{\mu}$ are 0.18 GPa. The background structure of the wave field, the analyzed frequency, and the interval of the grids for the discrete Fourier transform are the same as those for the previous numerical example.

Fig. 6(a) and (b) shows the amplitudes of the scattered waves in the $x_1 - x_2$ and $x_1 - x_3$ planes, respectively. According to Fig. 6 (a), the scattered waves are prominent in the regions where fluctuations of the medium are present. The regions for high amplitudes of the scattered waves are found to be separated due to the locations for the fluctuations of the medium. Therefore, the effects of multiple scattering are not very significant here. The reflection of

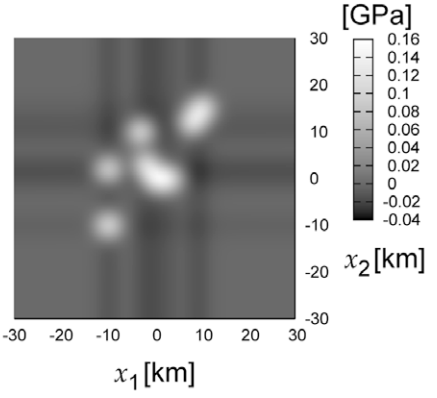

(a) Reconstruction of $\tilde{\lambda}$ in the $x_1 - x_2$ plane.

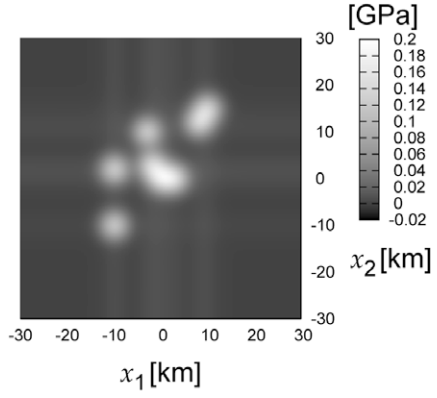

(b) Reconstruction of $\tilde{\mu}$ in the $x_1 - x_2$ plane.

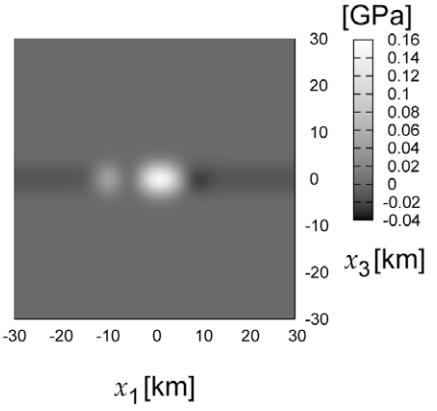

(c) Reconstruction of $\tilde{\lambda}$ in the $x_1 - x_3$ plane.

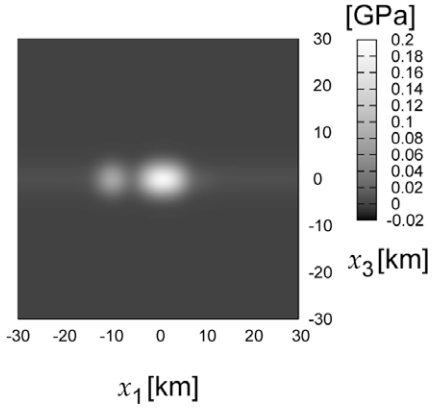

(d) Reconstruction of $\tilde{\mu}$ in the $x_1 - x_3$ plane.

Fig. 8. Results of the inverse scattering analysis due to smooth fluctuations.

the waves due to the incident wave is found to be small because of the smooth fluctuations. According to Fig. 6(b), forward scattering is noticeable with the narrow directionality in the x_3 direction. Interference of the scattered waves can be found in the far field range of regions of the fluctuation.

The spectral structure of the scattered waves in the $\xi_1 - \xi_2$ and $\xi_1 - \xi_3$ planes are shown in Fig. 6(c) and (d), respectively. According to Fig. 6(c), the scattered waves propagating in the $x_1 - x_2$ plane are produced by the *P* wave, and waves whose wavelength is longer than that of the *P* wave. In addition, the component of the *P*

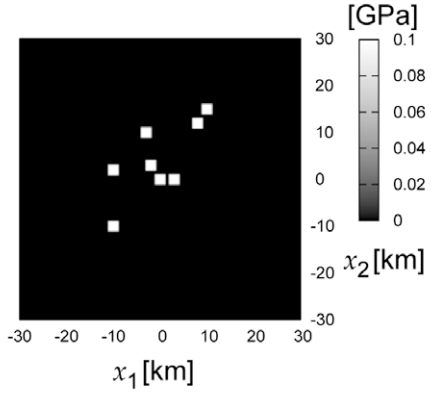

(a) Fluctuations of Lamé constants $\tilde{\lambda}$ and $\tilde{\mu}$ in the $x_1 - x_2$ plane.

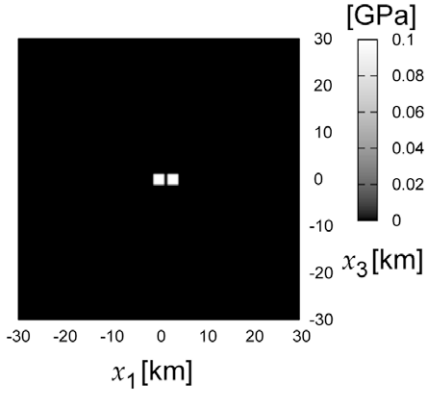

(b) Fluctuations of Lamé constants $\tilde{\lambda}$ and $\tilde{\mu}$ in the $x_1 - x_3$ plane.

Fig. 10. Analyzed model of discontinuous fluctuations.

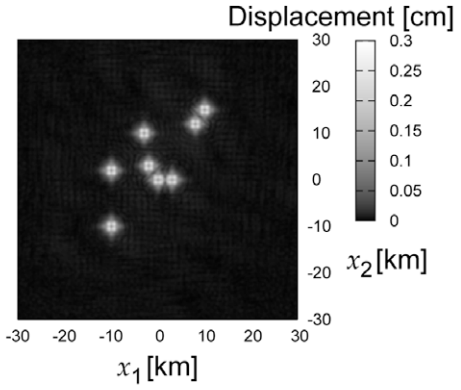

(a) Amplitudes of the scattered waves in the $x_1 - x_2$ plane.

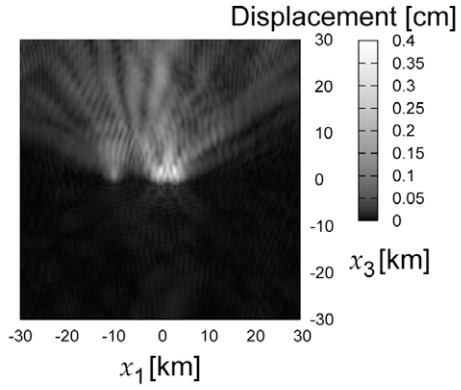

(b) Amplitudes of the scattered waves in the $x_1 - x_3$ plane.

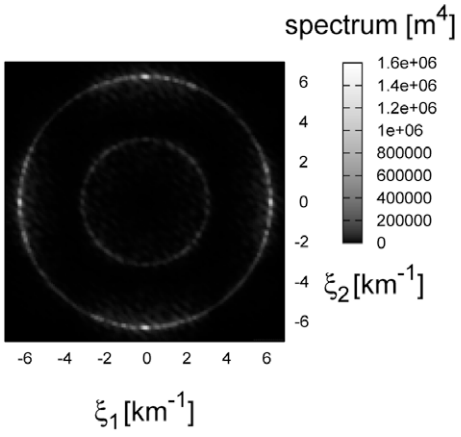

(c) Wavenumber spectrum of the scattered waves in the $\xi_1 - \xi_2$ plane.

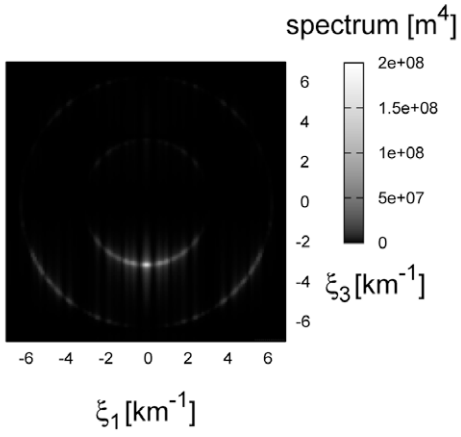

(d) Wavenumber spectrum of the scattered waves in the $\xi_1 - \xi_3$ plane.

Fig. 11. Results of the forward scattering analysis due to discontinuous fluctuations.

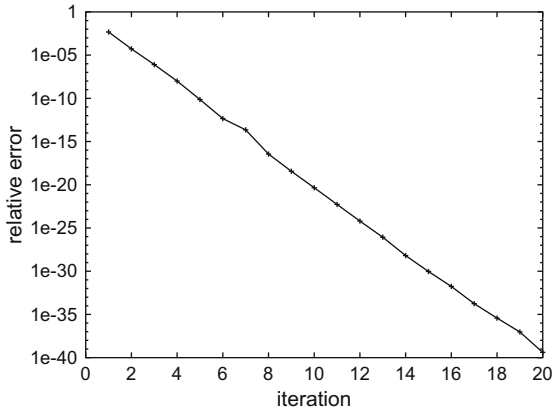

Fig. 12. Convergence of the solution for the forward scattering analysis due to discontinuous fluctuations by the Bi-CGSTAB method.

wave whose wavenumber is 3.14 km^{-1} is noticeable in Fig. 6(c). The reason is due to the fact that the incident wave is the *P* wave and the fluctuations of the medium are stiffer compared to the background structure. According to Fig. 6(d), the spectrum of the scattered waves in $\xi_1 - \xi_3$ plane is found to be localized in a very narrow region with a very high amplitude. The spectrum in this localized region describes a *P* wave propagating along the x_3 direction. This spectral structure helps to explain the properties of Fig. 6(b).

The convergence of solutions for the analysis based on the Bi-CGSTAB method is shown in Fig. 7. A rapid decrease in the relative error can be found in Fig. 7. The speed of the decrease in the relative error here is almost the same as the result shown in Fig. 4. Namely, only two iterations were required to make the relative error less than 1.0×10^{-5}.

The results of the inverse scattering analysis in the $x_1 - x_2$ and $x_1 - x_3$ planes are shown in Fig. 8. For the analysis, ϵ for expressing ∂_2^{-1} and $(\partial_3 + ik_L)^{-1}$ in the operator M_{jk} was set to 0.01. It is seen from Fig. 8 that the amplitudes and the locations for the fluctuations were successfully reconstructed from the scattered wave field. Namely, Eq. (77) is effective and available for the inverse scattering analysis in the case where the whole of the scattered wave field is provided. Fig. 9 shows the convergence of the relative error during the inverse scattering analysis. For a comparison, the GCR method is also employed for the analysis. It is found from Fig. 9 that the Bi-CGSTAB method does not show very good convergence properties after several iterations, when compared to the GCR method. Therefore, it would be convenient for us to have several alternative iterative methods for the analysis by means of the present method.

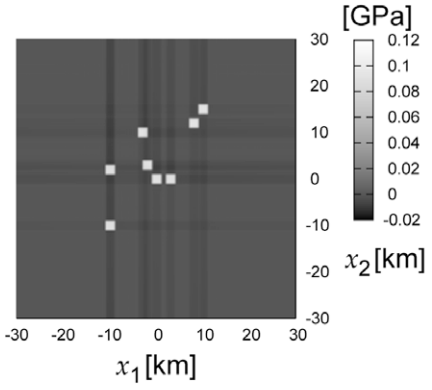

(a) Reconstruction of $\tilde{\lambda}$ in the $x_1 - x_2$ plane.

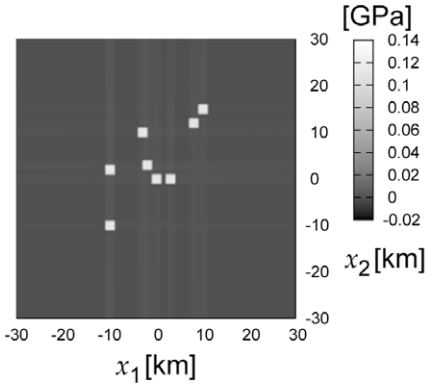

(b) Reconstruction of $\tilde{\mu}$ in the $x_1 - x_2$ plane.

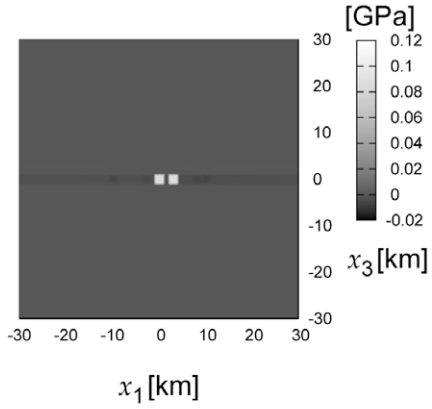

(c) Reconstruction of $\tilde{\lambda}$ in the $x_1 - x_3$ plane.

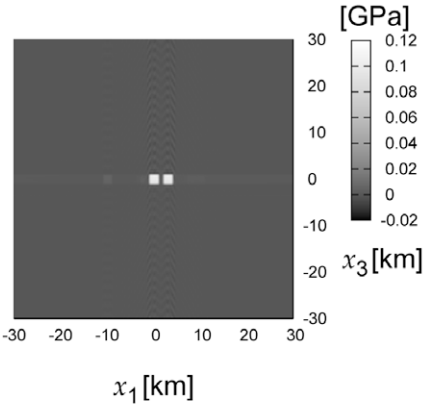

(d) Reconstruction of $\tilde{\mu}$ in the $x_1 - x_3$ plane.

Fig. 13. Results of the inverse scattering analysis due to discontinuous fluctuations.

3.3. Analysis of multiple scattering due to discontinuous fluctuations

Finally, a multiple scattering problem due to discontinuous fluctuations is investigated. The analyzed model is shown in Fig. 10, in which the fluctuations of the medium are determined by several cubes, and the incident P wave propagates along the x_3 axis. The expression for the fluctuations is given by

$$\begin{aligned}\tilde{\lambda}(x) &= \sum_{i=1}^{N_f} A_{\lambda_i}\chi_{Q_i}(x)\\ \tilde{\mu}(x) &= \sum_{i=1}^{N_f} A_{\mu_i}\chi_{Q_i}(x), \quad (x \in \mathbb{R}^3)\end{aligned} \tag{84}$$

where N_f is the number of cubes, A_{λ_i} and A_{μ_i} are the amplitudes of the fluctuations for the Lamé constants $\tilde{\lambda}$ and $\tilde{\mu}$, respectively, and χ_{Q_i} is the characteristic function defined by

$$\chi_{Q_i}(x) = \begin{cases} 1 & \text{when } x \in Q_i \\ 0 & \text{when } x \notin Q_i \end{cases} \tag{85}$$

Note that Q_i in Eq. (85) denotes a cubical region in $\mathbb{R}^3$.

For the analysis, the background Lamé constants, the intervals, the number of grid points in the space and the wavenumber domain, the analyzed frequency, the amplitude of the incident P wave, and ϵ for Green's function are the same as those in the previous numerical example. The amplitude of the fluctuation in the cubes is 0.1 GPa. As can be seen in Eq. (9), the derivative of the Lamé constants are required for the volume integral equation. The spatial derivatives of the Lamé constants are approximated by the discrete Fourier transform as shown in Eq. (40).

The results of the forward scattering analysis are shown in Fig. 11(a) and (b). The amplitudes of the scattered waves in the $x_1 - x_2$ and $x_1 - x_3$ planes are presented here. According to Fig. 11(a), the scattered waves can be seen mostly in the regions where the fluctuations are present. The high amplitudes regions for the scattered wave field are almost separated due to the locations for the fluctuations of the medium. This shows that the reflections of the waves at the surface boundaries of the cubes are not very strong. In particular, the effects of multiple scattering are not very significant here. It is found from Fig. 11(b) that the amplitudes for the forward scattering are noticeable in the $x_1 - x_3$ plane. The directionality of forward scattering is wider compared to the results due to the smooth fluctuations shown in Fig. 6(b). The reason for this is that the scattered waves are caused not only by the surfaces on the forward side, but also at the corners of the cubes. Note that the size of the cubes for the current analysis is small compared to the wavelength of the wave field. Therefore, the amplitude itself for the scattered waves is smaller compared to the previous results shown in Fig. 6(a) and (b). Due to the same reason, the effects of multiple scattering as well as those of backward scattering are small.

The spectral structure of the scattered waves in the $\xi_1 - \xi_2$ and $\xi_1 - \xi_3$ planes are shown in Fig. 11(c) and (d), respectively. According to Fig. 11(c), the wavenumber for the S wave, (i.e., 6.28 km^{-1}), is found to be prominent. Namely, the scattered waves propagating in the $x_1 - x_2$ plane are almost the S wave itself. Those waves are caused by the incident P wave on the lateral surfaces of the cubes. On the other hand, the wavenumber for the P wave is prominent in the $\xi_1 - \xi_3$ plane. Therefore, the scattered waves on the forward side in the $x_1 - x_3$ plane are found to be P waves. The spread of the spectrum for the P wave in Fig. 11(d) explains the wide directionality of the propagation of the scattered waves The relation between the relative error and the iteration number during the iterative process for solving the forward problem is shown in Fig. 12, in which a rapid decrease in the relative error can also be seen.

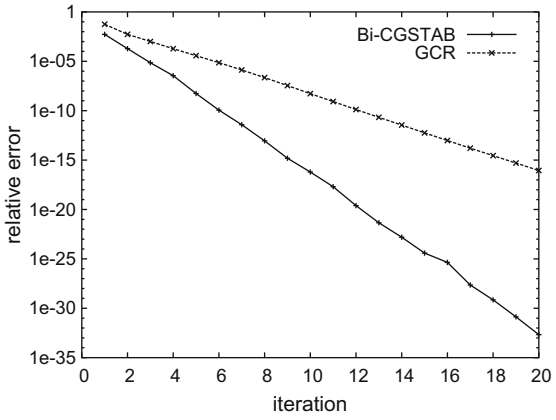

Fig. 14. Convergence of the solution for the inverse scattering analysis due to discontinuous fluctuations.

The results of the inverse scattering analysis are shown in Fig. 13 for the $x_1 - x_2$ and $x_1 - x_3$ planes. It is found in Fig. 13 that the locations and amplitudes for the fluctuations of the medium are successfully reconstructed. Therefore, the current method is effective even for the identification of discontinuous fluctuations of the wave field if the whole of the scattered wave field is provided. The convergence of the solution during the iterative process is shown in Fig. 14. The convergence properties are compared by the Bi-CGSTAB and GCR methods. The convergence properties for both Bi-CGSTAB and GCR are very good. Note that the convergence properties of the Bi-CGSTAB method in Fig. 14 are found to be better than those in Fig. 9. One of the reasons for this is that the amplitudes and spreads of the scattered wave field due to the smooth fluctuations were larger than those of the current wave field.

For inverse scattering analysis in a practical situations, the whole of the scattered wave field is approximated from the limited observed data. Further investigations and discussions would be required in the future for inverse scattering analysis. For example, estimations of the wave field by means of the far field patterns and asymptotic expansion would be necessary for the volume integral equation in these situations.

For both the forward and inverse scattering analysis, the required CPU time depends on the number of grid points in $\mathbb{R}^3$, the number of iterations, and the employed solver. Throughout the numerical calculations in this paper, the CPU time was only 2 min if the Bi-CGSTAB method and two iterations were adopted.

4. Conclusion

A fast method for the volume integral equation applicable to both forward and inverse scattering analysis has been developed in this paper. The starting point of the formulation was the volume integral equation in the wavenumber domain. The discrete Fourier transform resolved the problem of the differential operations required in the volume integral equation and as a result a non-Hermitian linear operator on a finite dimensional vector space was defined and utilized. The Bi-CGSTAB method and FFT were applied to solve the integral equation in the wavenumber domain. The calculation of a coefficient matrix, which consumes vast amounts of memory, was not necessary. The mathematical advantage of the volume integral equation in the wavenumber domain was that it directly showed the relation between the fluctuation of the medium and the scattered wave field. The formulation for inverse scattering analysis made use of this. The shift operator was introduced into the integral equation for inverse scattering analysis to modify

the equation into a Fredholm equation of the second kind. According to the numerical examples, a fast and accurate method for the volume integral equation was established. For example, the CPU time to have accurate solutions was only 2 min. The reconstruction of inhomogeneities of the wave field was also successful even for multiple scattering of several cubes.

References

Barrett, R., Berry, M., Chan, T.F., Demmel, J., Donato, J., Dongarra, J., Eijkhout, V., Pozo, R., Romine, C., Van der Vorst, H., 1994. Templates for the solution of linear systems: building blocks for iterative methods. SIAM.

Colton, D., Kress, R., 1983. Integral Equation Methods in Scattering Theory. John Wiley and Sons, Inc., New York.

Colton, D., Kress, R., 1998. Inverse Acoustic and Electromagnetic Scattering Theory. Springer-Verlag, Berlin, Heidelberg.

De Zaeytijd, J., Bogaert, I., Franchois, A., 2008. An efficient hybrid MLFMA-FFT solver for the volume integral equation in case of sparse 3D inhomogeneous dielectric scatterers. Journal of Computational Physics 227, 7052–7068.

Fata, S.N., Guzina, B.B., 2004. A linear sampling method for near-field inverse problems in elastodynamics. Inverse Problems 20, 713–736.

Friedlander, F.G., Joshi, M., 1998. Introduction to the Theory of Distributions. Cambridge University Press.

Guzina, B.B., Fata, S.N., Bonnet, M., 2003. On the stress-wave imaging of cavities in a semi-infinite solid. International Journal of Solids and Structures 40, 1505–1523.

Guzina, B.B., Chikichev, I., 2007. From imaging to material identification: a generalized concept of topological sensitivity. Journal of Mechanics and Physics of Solids 55, 245–279.

Hörmander, L., 1983. The Analysis of Linear Partial Differential Operators I. Springer-Verlag, Berlin, Heidelberg.

Ikebe, T., 1960. Eigenfunction expansion associated with the Schroedinger operators and their applications to scattering theory. Archive for Rational Mechanics and Analysis 5, 1–34.

Kato, T., 1980. Perturbation Theory for Linear Operators. Springer-Verlag, Berlin, Heidelberg.

Kleinman, R.E., van den Berg, P.M., 1992. A modified gradient method for two-dimensional problems in tomography. Journal of Computational and Applied Mathematics 42, 17–35.

Reed, M., Simon, B., 1975. Method of Modern Mathematical Physics Fourier Analysis and Self-adjointness. Academic Press, San Diego. vol. II.

Touhei, T., 2009. Generalized Fourier transform and its application to the volume integral equation for elastic wave propagation in a half space. International Journal of Solids and Structures 46, 52–73.

Yang, J., Abubaker, A., van den Berg, P.M., Habashy, T.M., Reitich, F., 2008. A CG-FFT approach to the solution of a stress–velocity formulation of three-dimensional scattering problems. Journal of Computational physics 227, 10018–10039.